Effective thermal conductivity of oolitic rocks using the Maxwell homogenization method

Albert Giraud, I Sevostianov, F Chen, D Grgic

Effective thermal conductivity of oolitic rocks using the Maxwell homogenization method

A. Giraud[a,*], I. Sevostianov[b,c], F. Chen[a], D. Grgic[a]

[a] *GeoRessources Laboratory, Université de Lorraine (ENSG), CNRS, CREGU, F-54518 Vandoeuvre-lès-Nancy, France*
[b] *Department of Mechanical and Aerospace Engineering, New Mexico State University, Las Cruces, NM 88001, USA*
[c] *ITMO University, Kronverkskiy pr. 49, St. Petersburg 197101, Russia*

Abstract

The present work focuses on effective thermal conductivity of oolitic limestones, characterized by an assemblage of porous grains (oolites), mesopores and solid grains. Two distinct scales of pores, micropores or intra oolitic pores and mesopores or inter oolitic pores are taken into account. At the first step, micropores are homogenized inside the oolites by using self consistent homogenization scheme. The second homogenization step describing transition from the mesoscale to the macroscale, is performed by using a recent reformulation of the Maxwell homogenization scheme (see [1]). At the mesoscale, porous oolitic inclusions are quasi spherical whereas two families of mesopores are considered according to analysis of photomicrographs: (1) randomly oriented oblate spheroidal pores and (2) concave pores. The proposed model is compared to a simplified one when all the pores are of ellipsoidal shape. The relevancy of the ellipsoidal approximation is then evaluated. In particular, the influence of the shape of the mesopores on the overall thermal conductivity is discussed. Comparisons between multi-scale model based on Maxwell homogenization method and experimental data show that effects of porosity and saturating fluids on overall conductivity are correctly predicted when concave pores are taken into account.

Keywords: effective thermal conductivity, Maxwell homogenization method, oolitic limestone, two-scale porosity , concave pore

*Corresponding author
Email address: Albert.Giraud@univ-lorraine.fr (A. Giraud)

1. Introduction

The present work focuses on the determination of overall thermal conductivity of oolitic limestone that is modeled as a heterogeneous material composed by an assemblage of quasi-spherical porous grains (oolites, o), mesopores (b) and solid matrix (sparitic cement c) (see [2], [3], [4], [5]). For this goal, we use recently reformulated Maxwell's homogenization method for elastic composites [1] which was successfully applied to the estimate of effective elastic constants of oolitic. This method has also been explored in ([6], [7] , [8]) for mechanical properties and in ([9], [10]) for conductivity. It must be emphasized that Maxwell's homogenization model has been presented in [11] for the prediction of the thermal conductivity of fluid-saturated rocks. In particular, it has been shown in [11] that this model allows to predict overall thermal conductivity in a wide range of rock-microstructure type of sedimentary or cristalline rocks, by considering randomly distributed spheroidal pores.

One specific point related to the microstructure of heterogeneous oolitic porous rocks is the multiscale structure of pore space. The complex realistic pore structure can be simplified and the total porosity can be decomposed into two scale separated classes of pores: intra oolitic pores or micropores, at the micro scale, and inter oolitic pores or mesopores at the mesoscale. The microstructural model presented in [12] is adopted in this paper. The novelty of the model consists in the account for concave pores modelled by superspherical ones. Reformulation of Maxwell's homogenization method in terms of the resistivity contribution tensors allows accounting for non-ellipsoidal shape of such pores using the numerically evaluated contribution tensors (see [13]) when no analytical solution can be obtained. This model is then compared to a simple one in which the concave pores are replaced by the best ellipsoidal approximates.

Extensive study of the effective properties of carbonate rocks taking into account a multi-scale description, with applications to elasticity, electrical conductivity, thermal conductivity and permeability in the context of a cross property analysis have been presented by M. Markov and coauthors ([14], [15], [16], [17], [18]). In these works, two distinct classes of pores are considered: primary small scale pores and secondary mesoscopic pores. Small scale pores are similar to intra oolitic pores of oolitic rocks, and secondary

pores similar to inter oolitic pores. A very complete description of the secondary (large scale) porosity is presented in [14] by introducing four types of pores: vugs (quasi-spherical inclusions), quasi vugs (oblate ellipsoids), channels (prolate ellipsoids), and cracks (strongly oblate inclusions). The presence of an interphase coating oolites, an *Interfacial Transition Zone* (ITZ), is not taken into account in this paper but it is certainly important in porous oolitic rocks similarly to the cement based material (see for example [19] for a study of the influence of *Interfacial Transition Zone* on effective conductivity).
Among many papers related to characterization of thermal conductivity of porous heterogeneous rocks, [20] present an experimental characterization including a large sensitive study of physical parameters, in a wide temperature range. An extensive literature review on thermal conductivity measurements in carbonate rocks may be found in [21]. Importantly, overall isotropy of thermal conductivity is observed in most cases. The authors pointed out that anisotropic single crystals, including calcite, show directional differences in thermal conductivity, but randomly oriented polycrystalline aggregates produce an overall isotropic thermal effective conductivity. This result is consistent with the developed approach in the present paper. Random distribution of calcite phase mineral is accounted through averaging of the calcite mineral thermal conductivity (see [22]) and by using equivalent isotropic conductivity.
A detailed review of thermal conductivity data sets for geomaterials made of natural soil particles, crushed rock particles and sedimentary rock including analysis of influence of particle shape, grains pore-size distributions, fluid saturated (air and liquid water) is given in [23]. It may be noticed that [24] have recently studied thermal conductivity of gas saturated porous materials taking into account methods of statistical physics and rarefied gas dynamics. They have shown that in the slip flow regime corresponding to low Knudsen number, it is necessary to use the method of rarefied gas dynamics to correctly predict the effective thermal conductivity. These phenomena may be of major importance in nano-porous materials and porous rocks such as gas shales. In the present study we focused on the micro and meso porosities of oolitic limestones, respective pore size correspond to the standard hydrodynamic regime and these phenomena have been neglected.

2. Background results

Hereafter we define some notations and recall some results which are needed later. Upper case boldsymbols $\boldsymbol{P}$, $\boldsymbol{\Lambda}$, $\boldsymbol{I}$ refer to second order tensors, lower case boldsymbols, as $\boldsymbol{a}$, $\boldsymbol{\varepsilon}$, $\boldsymbol{\sigma}$, refer to first order tensors. $\boldsymbol{I}$ represents the second-order, identity tensor (δ_{ij} denotes Kronecker delta symbol, $\delta_{ij} = 1$ if $i = j$, $\delta_{ij} = 0$ otherwise). For the sake of simplicity only the polarisation tensors related to spheroidal inclusions are recalled. The general case of the $3D$ ellipsoid could be also considered in what follows. *Oblate spheroïd* ($0 < \gamma < 1$) and *prolate spheroïd* ($1 < \gamma$), with symmetry axis 3 are described by equation

$$\begin{aligned} &\boldsymbol{z} \in \Omega_I \Leftrightarrow \frac{z_1^2}{a^2} + \frac{z_2^2}{a^2} + \frac{z_3^2}{a^2\gamma^2} \leq 1 \quad , \quad 0 \leq \gamma \leq 1 \\ &a_1 = a_2 = a \quad , \quad a_3 = a\gamma \end{aligned} \tag{1}$$

Hill Polarisation tensor of a spheroidal inclusion in an infinite isotropic elastic medium (λ denotes the conductivity of the infinite isotropic medium surrounding the spherical inclusion) is a transversely isotropic second order tensor

$$\boldsymbol{P} = \frac{Q(\gamma)}{\lambda}\boldsymbol{I}_T + \frac{1 - 2Q(\gamma)}{\lambda}\boldsymbol{I}_N \tag{2}$$

$$\boldsymbol{I}_N = \boldsymbol{e}_3 \otimes \boldsymbol{e}_3 \quad , \quad \boldsymbol{I}_T = \boldsymbol{e}_1 \otimes \boldsymbol{e}_1 + \boldsymbol{e}_2 \otimes \boldsymbol{e}_2 \quad , \quad \boldsymbol{I} = \boldsymbol{I}_N + \boldsymbol{I}_T \tag{3}$$

with (see [25] p. 441, or [26] p. 406, among many others)

$$Q(\gamma) = \begin{cases} \dfrac{1}{2}\left[1 + \dfrac{1}{u}\left(1 - \dfrac{\gamma}{\sqrt{v}}\arctan\left(\dfrac{\sqrt{v}}{\gamma}\right)\right)\right] & \text{if} \quad \gamma < 1 \\ \dfrac{1}{3} & \text{if} \quad \gamma = 1 \\ \dfrac{1}{2}\left[1 + \dfrac{1}{u}\left(1 - \dfrac{\gamma}{2\sqrt{u}}\ln\left(\dfrac{\gamma + \sqrt{u}}{\gamma - \sqrt{u}}\right)\right)\right] & \text{if} \quad \gamma > 1 \\ v = 1 - \gamma^2 \quad , \quad u = \gamma^2 - 1 & \end{cases} \tag{4}$$

Hill Polarisation tensor of a spherical inclusion ($\gamma = 1$ and $Q = 1/3$)

$$\boldsymbol{P} = \frac{1}{3\,\lambda}\,\boldsymbol{I} \tag{5}$$

$\boldsymbol{Q}$ tensor (see [27] equation 2.9) for Maxwell homogenization scheme

$$\boldsymbol{Q} = \boldsymbol{\Lambda}.\left(\boldsymbol{I} - \boldsymbol{P}.\boldsymbol{\Lambda}\right) \tag{6}$$

In the case of a sphere (using 5 and $\boldsymbol{\Lambda} = \lambda \boldsymbol{I}$)

$$\boldsymbol{Q} = \frac{2}{3}\,\lambda \boldsymbol{I} \tag{7}$$

Conductivity contribution tensor (see [10])

$$\boldsymbol{N}_i = \left[\boldsymbol{P} + \left(\boldsymbol{\Lambda}_i - \boldsymbol{\Lambda}\right)^{-1}\right]^{-1} \tag{8}$$

Resistivity contribution tensor (see [10])

$$\boldsymbol{H}_i = -\boldsymbol{\Lambda}^{-1}.\boldsymbol{N}_i.\boldsymbol{\Lambda}^{-1} \tag{9}$$

Dilute concentration tensor

$$\boldsymbol{A}_i = \left[\boldsymbol{I} + \boldsymbol{P}.\left(\boldsymbol{\Lambda}_i - \boldsymbol{\Lambda}\right)\right]^{-1} \tag{10}$$

In this paper, the reformulation of the Maxwell homogenization scheme in terms of resistivity contribution tensor (9) will be used. For a spherical inclusion i (λ_i) embedded in an infinite isotropic matrix

$$\boldsymbol{N}_i = N_i\ \boldsymbol{I} \quad , \quad \boldsymbol{H}_i = H_i\ \boldsymbol{I} \quad , \quad \boldsymbol{A}_i = A_i\ \boldsymbol{I} \tag{11}$$

$$A_i = \frac{3\lambda}{2\lambda + \lambda_i} \tag{12}$$

and

$$H_i = \frac{\lambda - \lambda_i}{\lambda^2} A_i \quad , \quad \overline{N}_i = -\left(\lambda - \lambda_i\right) A_i \tag{13}$$

In the case of an isotropic ellipsoidal inclusion with conductivity tensor $\boldsymbol{\Lambda}_i = \lambda_i \boldsymbol{I}$ surrounded by an infinite isotropic matrix with conductivity tensor $\boldsymbol{\Lambda} = \lambda \boldsymbol{I}$ (1) relation (5) gives

$$\boldsymbol{A}_i = \lambda \left(\frac{1}{\lambda\left(1 - Q(\gamma)\right) + \lambda_i Q(\gamma)} \boldsymbol{I}_T + \frac{1}{2\lambda Q(\gamma) + \lambda_i\left(1 - 2Q(\gamma)\right)} \boldsymbol{I}_N \right) \tag{14}$$

Orientational average (case of a random orientation distribution)

$$\overline{\boldsymbol{a}} = \frac{1}{3} Tr\left(\boldsymbol{a}\right) \ \ \boldsymbol{I} \tag{15}$$

One obtains spherical (isotropic) second order tensors

$$\overline{\boldsymbol{A}}_i = \overline{A}_i \boldsymbol{I} \quad , \quad \overline{\boldsymbol{H}}_i = \overline{H}_i \boldsymbol{I} \tag{16}$$

with

$$g\left(\lambda, \lambda_i, \gamma\right) = \frac{\lambda}{3} \left(\frac{2}{\lambda\left(1 - Q(\gamma)\right) + \lambda_i Q(\gamma)} + \frac{1}{2\lambda Q(\gamma) + \lambda_i \left(1 - 2Q(\gamma)\right)} \right) \tag{17}$$

$$\overline{A}_i = g\left(\lambda, \lambda_i, \gamma\right) \tag{18}$$

One verifies relations

$$\overline{H}_i = \frac{\lambda - \lambda_i}{\lambda^2} \overline{A}_i \tag{19}$$

3. Microstructure of a reference porous oolitic limestone

One presents in this section some microstructural observations of a reference porous oolitic rock chosen for this work, an oolitic limestone from Lavoux (West of France, see [28]) whose microstructure has been detailed [29]. One may also refers to [4], [2], for details. Oolites are quasi spherical grains constituted by concentric porous layers. The oolite microstructure are constituted by an assemblage of calcite grains (micrite, solid grains with diameter range $1\mu m - 5\mu m$) and micropores. More precisely oolites contain quasi spherical grains composed of concentric layers, diameter range $100\mu m - 1mm$, the layers are composed by an assemblage of micropores and micrite grains. Micrite or *microcristalline calcite* is composed spherical grains constituting solid oolitic phase, diameter range $1\mu m - 5\mu m$. Sparitic calcite cement or sparite, spar calcite, diameter range $20\mu m - 100\mu m$, it corresponds to the solid phase at the mesoscale. Solid phase of Lavoux limestone, i.e. micritic grains inside oolites and sparitic cement between oolites, is a quasi mono-mineral material constituted of pure calcite (solid volume fraction of calcite, $f^s_{calcite} = \Omega_{calcite}/\Omega_s \approx 0.98$).
The total pore volume fraction of Lavoux limestone varies from 0.15 to 0.30,

it is decomposed into two classes of pores: inter oolitic pores(mesopores) and intra oolitic pores (micropores) of approximately equal partial porosities [2]. As in [29], a sensitive study is performed in this paper on a relatively wide range of porosity. Mesoscopic pores are divided into two types of pores: oblate spheroidal pores of aspect ratio $\gamma = 0.2$ (index $b1$ in what follows) and ellipsoidal pores (index $b2$) replacing superspherical concave pores taken into account in [29].
Two cases are considered, flat pores similar to cracks are represented by oblate spheroidal pores of aspect ratio $\gamma = 0.05$, and elongated pores cracks are represented by prolate spheroidal pores of aspect ratio $\gamma = 20$. The partial porosities of the two kind of pores are assumed equal. Flat and elongated pores may respectively correspond to particular cases of secondary pores of carbonate rocks described in [14]: channels (prolate ellipsoids, as elongated pores), and cracks (flat oblate ellipsoids).
At the macroscopic level, experimental characterizations of the Lavoux limestone show that the overall elastic behaviour is not far from isotropy. It results from an isotropic or random distribution of constituents: oolites, sparitic cement and mesopores. Thermal conductivity needs to be measured on this reference material (and experimental study is currently performed and results will be presented in a next paper), and it is assumed that the overall conductivity is also isotropic. See [21] for an extensive review on thermal conductivity of carbonate rocks which confirms reasonably overall isotropy in most cases. The thermal conductivity of the pure calcite mineral will be assumed equal to $\lambda_c = 3.3\, W\, m^{-1}\, K^{-1}$ (according to [30] and [31]). The numerical values of thermal conductivities for liquid and air are respectively $\lambda_\ell = 0.5984\ W\ K^{-1}\ m^{-1}$ and $\lambda_g = 0.0255\ W\ K^{-1}\ m^{-1}$ (according to [32]).

3.1. Volume fractions and constituents

As in [2]-[29] three different scales may be identified. First the smallest scale, referred as *microscopic scale*, corresponds to the *intra granular* or *intra oolitic* level. Second the intermediate scale, referred as as *mesoscopic scale*, corresponds to the scale of oolite grains, syntaxial calcite grains (referred as sparitic calcite cement, and *inter oolitic* pores. Third the largest scale, referred as *macroscopic scale* corresponds to a large representative volume elements compared to the oolite size, interoolitic pores and syntaxial calcite grains. At the meso scale, one considers a four phase composite material composed of poroelastic oolites (o) (constituted by solid grains and *intra*

oolitic pores, or *micro pores*), inter oolitic meso pores divided into two families $b1$ and $b2$, and *sparitic cement* (or *syntaxial calcite*) constituted by pure calcite grains (index c).
A two scale porosity is considered as two population of voids may be identified. *Intra oolitic voids* of spherical or ellipsoidal shape, with average diameter of $0.1\,\mu m$, referred as *micropores* in what follows, with index a. *Inter oolitic voids* of ellipsoidal shape, with average diameter approximately of $10\,\mu m$, referred as *mesopores* b, divided into two families of equal volume fraction, indexes $b1$ and $b2$. The total volumes occupied by the phases write

$$\Omega = \Omega_o + \Omega_b + \Omega_c \tag{20}$$

with

$$\Omega_b = \Omega_{b1} + \Omega_{b2} \tag{21}$$

one have

$$\Omega = \Omega_o + \Omega_{b1} + \Omega_{b2} + \Omega_c \tag{22}$$

with corresponding volume fractions

$$\begin{aligned} &f_o = \frac{\Omega_o}{\Omega} \quad , f_{b1} = \frac{\Omega_{b1}}{\Omega} \quad , f_{b2} = \frac{\Omega_{b2}}{\Omega} \quad , f_c = \frac{\Omega_c}{\Omega} \\ &f_o + f_{b1} + f_{b2} + f_c = 1 \end{aligned} \tag{23}$$

One defines the total volume of *intra oolitic* pores

$$\Omega_o = \Omega_a + \Omega_o^s \tag{24}$$

and the porosity of the oolite phase at the mesoscopic scale

$$f_a = \frac{\Omega_a}{\Omega_o} \tag{25}$$

The total pore volume can be expressed as

$$\Omega_p = \Omega_a + \Omega_{b1} + \Omega_{b2} \tag{26}$$

and the total porosity

$$f_p = \frac{\Omega_a}{\Omega} + \frac{\Omega_{b1}}{\Omega} + \frac{\Omega_{b2}}{\Omega} = f_a f_o + f_{b1} + f_{b2} \tag{27}$$

Representative data for the reference material studied in this paper are close to $f_p = 0.26$, $f_o = 0.74$, $f_a f_o = 0.14$, $f_a = 0.19$, $f_b = 0.12$ (see [2]) but a sensitivity study will be performed on the volume fractions of the different phases.
In sensitive study, as in [29] we will consider $f_{b1} = f_{b2} = f_b/2$

4. A two-scale porosity model for effective thermal conductivity of isotropic porous oolitic rocks

4.1. First step: homogenization of micropores and solid grains inside oolites

The first step represents the transition from the microscopic scale to the mesoscopic scale. Oolite pores are homogenized and the result of the first step is the *porous oolite*.

As previously indicated, the granular and random microstructure of oolites conduces to choose the self consistent approximation, originally due to [33], for the step I. By respectively denoting λ_o^I, λ_a, λ_o conductivity of the oolite at the mesoscale, conductivity of the intra oolitic porous phase, conductivity of micritic solid grains ($\lambda_o = \lambda_c$), the well known self consistent approximations for a two phase material with spherical particles is the positive root of the quadratic equation (see [25] formula 18.13 p. 463)

$$\frac{f_a \lambda_a}{\lambda_a + 2\lambda_o^I} + \frac{(1-f_a)\,\lambda_o}{\lambda_o + 2\lambda_o^I} - \frac{1}{3} = 0 \tag{28}$$

It's well known solution writes (see [25] formula 18.14 p. 463, with $d = 3$, $f_2 = 1 - f_1$)

$$h(\lambda_1, \lambda_2, f_1) = \frac{1}{4}\left(\alpha_{12} + \sqrt{\alpha_{12}^2 + 8\lambda_1\lambda_2}\right) \tag{29}$$

$$\alpha_{12} = \lambda_1(3f_1 - 1) + \lambda_2(2 - 3f_1) \tag{30}$$

and then self consistent approximation writes

$$\lambda_o^I = h(\lambda_a, \lambda_o, f_a) \tag{31}$$

It may be noticed that, in the tested range of microporosity $f_a < 0.2$, as we consider spherical particles, numerical differences between Self Consistent approximation, and other approximations such as Maxwell or Mori Tanaka would not be very significant. In the present model, the impact on overall thermal conductivity is limited when compared to the second homogenization step which corresponds to the mesoscopic scale. This comment is restricted to the tested range of microporosity and it would be irrelevant for a wider range.

4.2. Second step: transition from the mesoscopic scale to the macroscopic scale with ellipsoidal pores

At the mesoscale one considers a four phase phase heterogeneous medium, which is composed of porous oolites, nearly spherical and randomly distributed, it is the main phase ($f_o \approx 0.74$ in the reference case), pure solid calcite referred as sparitic cement (index c), meso pores modelled as two distinct families of ellipsoids randomly distributed in orientation. Reformulation of Maxwell homogenization scheme recently by I. Sevostianov and coauthors in the context of elasticity and conductivity problems (see [27], [29], [7] , [8] , [9], [10]) is then used for the transition from the mesoscopic scale to the macroscopic scale. More precisely reformulation of Maxwell homogenization scheme in terms of resistivity contribution tensor provides (see [29] relation 10 using compliance contribution tensor) the simple scalar relation established under assumption of macro isotropy

$$\lambda_{\mathrm{MX}}^{\mathrm{eff}} = \left(\frac{1}{\lambda_c} + \left(\left(f_{b1}\overline{H}_{b1} + f_{b2}\overline{H}_{b2} + f_o H_o \right)^{-1} - \frac{2}{3}\lambda_c \right)^{-1} \right)^{-1} \tag{32}$$

with $\overline{H}_{b1}$, $\overline{H}_{b2}$ and H_o respectively given by formula (19-13)

$$\overline{H}_{b1} = \frac{\lambda_c - \lambda_b}{\lambda_c^2} g\left(\lambda_c, \lambda_b, \gamma_{b1}\right) \quad , \quad \overline{H}_{b2} = \frac{\lambda_c - \lambda_b}{\lambda_c^2} g\left(\lambda_c, \lambda_b, \gamma_{b2}\right) \tag{33}$$

$$H_o = \frac{3\left(\lambda_c - \lambda_o^I\right)}{\lambda_c\left(2\lambda_c + \lambda_o^I\right)} \tag{34}$$

From relation (32) one may easily deduce an explicit formula for the effective thermal conductivity

$$\lambda_{\mathrm{MX}}^{\mathrm{eff}} = \lambda_c \frac{3 - 2\lambda_c\left(f_{b1}\overline{H}_{b1} + f_{b2}\overline{H}_{b2} + f_o H_o\right)}{3 + \lambda_c\left(f_{b1}\overline{H}_{b1} + f_{b2}\overline{H}_{b2} + f_o H_o\right)} \tag{35}$$

It should be emphasized that a more complex description of the mesoscale porosity could be easily introduced in the reformulation of Maxwell homogenization scheme in terms of resistivity contribution. As an example, the fourth types of secondary pores distinguished in [14] for carbonate rocks

could be introduced as randomly oriented spheroids are considered and relation (32) would be replaced by

$$\lambda_{\mathrm{MX}}^{\mathrm{eff}} = \left(\frac{1}{\lambda_c} + \left(\left(f_{b1}\overline{H}_{b1} + f_{b2}\overline{H}_{b2} + f_{b3}\overline{H}_{b3} + f_{b4}\overline{H}_{b4} + f_o H_o \right)^{-1} - \frac{2}{3}\lambda_c \right)^{-1} \right)^{-1} \quad (36)$$

f_{bi} and $\overline{H}_{bi}$ respectively denoting volume fraction and resistivity contribution tensor of the mesoscale pore bi. As oolites are not perfectly spherical, a random distribution of the best ellipsoidal approximation of oolites (oblate spheroids with aspect ratio close to $\gamma = 0.7$) could be also used and relation (32) would be replaced by

$$\lambda_{\mathrm{MX}}^{\mathrm{eff}} = \left(\frac{1}{\lambda_c} + \left(\left(f_{b1}\overline{H}_{b1} + f_{b2}\overline{H}_{b2} + f_o \overline{H}_o \right)^{-1} - \frac{2}{3}\lambda_c \right)^{-1} \right)^{-1} \quad (37)$$

with $\overline{H}_o$ given by a relation similar to (33). In further works we will also take into account more realistic shapes such as concave shapes (see recent paper [13]). As previously indicated, ellipsoidal shape is adopted for simplicity and in this case the best ellipsoidal approximation of more complex shapes needs to be used.

It may be noticed that relations (32-36-32) are very similar to relation 4.9 of paper [27], and relations $13 - 17$ of paper [29], which have been obtained in elasticity.

4.3. Second step: transition from the mesoscopic scale to the macroscopic scale with concave pores

As in [29], concave pores ($b2$) are approximated by superspheres

$$(|x|)^{2p} + (|y|)^{2p} + (|z|)^{2p} = 1 \quad (38)$$

of concavity factor $p = 0.35$ (see figure 4) For pores of the shape of supersphere of concavity factor p, approximate expressions for components of the resistivity contribution tensor have recently be obtained by [13] (see [34] for the elasticity problem) thanks to a numerical method (Finite Element Method). As this tensor is spherical (hydrostatic) one have

$$\overline{H}_{b2} = H_{b2} \quad (39)$$

Numerical values of the resistivity contribution tensors are given in the next section, as they depend on the thermal conductivity of the surrounding matrix (λ_c) and the inclusion (liquid water and air will be considered).

5. Numerical results

5.1. Experimental data

We present in this section a comparison of the developed micro-macro model with experimental results for relatively pure calcitic limestones presented in [35]. Oolitic limestones studied in this paper belong to this type of limestone. Intra oolite solid grains and inter oolite sparitic cement are composed of calcite. Extensive bibliographical review and data relative to thermal conductivity of limestones may be found in [20], [36], and in [11] for porous rocks more generally. Experimental results are presented in figures (5-6) and they cover a wide range of porosity (upper porosity is close to 0.7 which corresponds to highly porous rocks). In this paper, we restrict the study to the range $0 \leq f_b \leq 0.3$ which is relatively large for oolitic limestones. Upper value of thermal conductivity is given by the conductivity of the calcitic solid phase and it corresponds to the case of zero porosity. As expected, as conductivities of air and liquid water are lower than that of solid, effective thermal conductivity decreases with increasing values of porosity. In both cases, pore space respectively fully saturated by air or liquid water, effective thermal conductivity - porosity curve may be accurately fitted by a linear function of porosity (see figures 5-6). As experimental data collected in bibliographical review are not restricted to the detailed investigated microstructure type (oolitic limestone rocks with two-scale porosity), the aim of the comparison is not to very accurately fit the data but mainly to recover qualitative results, in particular effects of porosity and saturating fluid on overall thermal conductivity.

5.2. Simplified model based on ellipsoidal approximation for all pore families

The sensitive study is similar to the one presented in [29]. For the simplified model based on ellipsoidal approximation, mesopore family $b2$ is modelled by flat oblate pores close to cracks ($\gamma = 0.05$) or elongated prolate pores ($\gamma = 20$) instead of concave pores of superspherical shape.
Two cases are considered: porosity fully saturated with liquid water ($\lambda_\ell = 0.5984\, W\, m^{-1}\, K^{-1}$), *wet case*, and porosity fully saturated with air ($\lambda_a = 0.0255\, W\, m^{-1}\, K^{-1}$), *dry case*.
Figures (7-8-9-10) illustrate dependence of the effective thermal conductivity on the mesoporosity (assuming that $b1$ and $b2$ pore families have the same volume fractions) at different levels of the volume fraction of oolites ($f_o = 0.4 - 0.5 - 0.6 - 0.7$).

As it has been observed in elasticity [29], distribution of the volume concentration between spar calcite and porous oolitic grains plays minor role as compare to volume fraction of pores.
As expected, to the higher conductivity contrast between solid calcite mineral and air:

$$\frac{\lambda_c}{\lambda_g} \approx 129.4 \tag{40}$$

compared to the corresponding ratio between solid calcite and liquid water

$$\frac{\lambda_c}{\lambda_\ell} \approx 5.5 \tag{41}$$

the higher impact of the porosity on the overall thermal conductivity is observed in the *dry case*. Due to this higher contrast, the case of the air saturated porosity the most interesting for a micro-macro characterization because it is more sensitive to pore shape than the case of water liquid saturated (air saturated porosity is similar to an insulating phase). Comparisons between model and experiments show that flat oblate spheroidal pores ($\gamma = 0.05$) overestimate the effect of porosity on the overall in the case of air saturated pores. This overestimate is less pronounced in the case of liquid saturated pores. In both cases, liquid and air, prediction of model are more accurate with prolate spheroidal elongated pores ($\gamma = 20$) than crack similar oblate pores.

5.3. Model including concave pores family

One only replaces ellipsoidal pore family $b2$ by superspheres of concavity factor $p = 0.35$ and the same sentivity study is performed. Preceding values of resistivity contribution tensor (formula 33) needs to be replaced by the following numerical values (see [13] for details on calculation of resistivity contribution tensors).

$$\overline{H}_{b2}^{\text{supersph}}(\lambda_c, \lambda_\ell) = 0.447518 \tag{42}$$

$$\overline{H}_{b2}^{\text{supersph}}(\lambda_c, \lambda_g) = 0.528849 \tag{43}$$

and relation (35) can be used. Figures (11-12) illustrate dependence of the effective thermal conductivity on the mesoporosity at different levels of the volume fraction of oolites. Comparison with experimental data show that the model accurately predicts effect of porosity and effect of saturating fluid. Similarly to the model with prolate elongated pores, variations of effective thermal conductivity with porosity in the most sensitive case of air saturated porosity are correctly reproduced. Microstructural observations (see figure 4) show that concave pore shapes are more relevant than elongated pore shapes to describe the mesopores filling the space between spherical oolites. Experimental data correspond to purely calcitic limestones, and it is not restricted to oolitic limestones. A more accurate validation of the model by comparison with experimental data specific to oolitic limestone will be necessary. Experimental study of effective thermal conductivity of Lavoux oolitic limestone is in progress and experimental results will be presented in a next paper.

On the basis of the preceding results, a best ellipsoidal approximation can be proposed for this material by minimising the difference between the numerical values of the resistivity contribution tensor respectively obtained for the supersphere (43-42) and for the spheroids (33), for the two cases (air saturated and water liquid saturated)

$$\gamma_{b2}^{\text{Air-min}} \approx 0.31 \tag{44}$$

$$\gamma_{b2}^{\text{Lq-min}} \approx 0.11 \tag{45}$$

Resistivity contribution tensor of a superspherical inclusion depends on the shape parameter (concavity parameter p) and on the contrast between respective thermal conductivities of inclusion and matrix. This contrast is

very different in the two extreme cases investigated (see 40-41). As a consequence, the best ellipsoidal approximation depends on the conductivities of constituents, and it yields different aspect ratii in the two cases

6. Conclusion

The main factor affecting elastic properties of oolitic limestone is the pore space geometry. As identified in [29] some mesopores are concave and may be approximated by superspherical shape (see [34], [13]). A simplified model is presented by using ellipsoidal approximation for all the pores. This model could be used as a first approach for estimating overall thermal conductivity, its advantage being the simplicity of the corresponding homogenization model. Numerical results confirms the potential importance of the shape of mesopores for the conductivity problem (see [29]). In the two particular cases presented: air saturated and liquid water saturated pores, the comparison between resistivity contribution tensors of spheroids allows to define, in each case the best ellipsoidal approximation for a given superspherical shape.
Comparison between multi-scale model based on Maxwell homogenization method and experimental data show that it correctly predicts effects of porosity and saturating fluid on overall thermal conductivity, when taking into account concave pore of superspherical shape. These results are interesting in relation to cross property analysis between elastic coefficients and thermal conductivity. It confirms previous results obtained with a similar upscaling model for the same material, for the prediction of elastic coefficients [12]. Experimental characterization of the thermal conductivity of such oolitic limestones, at different saturation ratios is also in progress and comparison with numerical results needs to be performed.

Acknowledgement

Financial support from the from TAMER European project(Trans-Atlantic Micromechanics Evolving Research Materials containing inhomogeneities of diverse physical properties, shapes and orientations), FP7 Project TAMER IRSES-GA-2013-610547, New Mexico Space Grant Consortium contained in the NASA Cooperative Agreement NNX13AB19A to New Mexico State University, and NSF grant DMR-1229558 are gratefully acknowledged.

7. References

[1] I. Sevostianov, A. Giraud, Generalization of Maxwell homogenization scheme for elastic material containing inhomogeneities of diverse shape, International Journal of Engineering Science 64 (1) (2013) 23 – 36.

[2] A. Giraud, N. B. Nguyen, D. Grgic, Effective poroelastic coefficients of isotropic oolitic rocks with *micro* and *meso* porosities, International Journal of Engineering Science 58 (2012) 57–77.

[3] D. Grgic, The influence of CO_2 on the long-term chemo-mechanical behavior of an oolitic limestone, Journal of Geophysical Research 116 (B7) (2011) 2156–2202.

[4] N. B. Nguyen, A. Giraud, D. Grgic, A composite sphere assemblage model for porous oolitic rocks, International Journal of Rock Mechanics and Mining Sciences 48 (2011) 909–921.

[5] S. Ghabezloo, J. Sulem, S. Guédon, F. Martineau, Effective stress law for the permeability of a limestone, International Journal for Rock Mechanics and Mining Science 46 (2009) 297–306.

[6] V. Levin, S. Kanaun, M. Markov, Generalized Maxwell's scheme for homogenization of poroelastic composites, International Journal of Engineering Science 61 (1) (2012) 75 – 86.

[7] I. Sevostianov, On the shape of effective inclusion in the Maxwell homogenization scheme for anisotropic elastic composites, Mechanics of Materials 75 (0) (2014) 45 – 59.

[8] I. Sevostianov, V. Levin, E. Radi, Effective properties of linear viscoelastic microcracked materials: Application of Maxwell homogenization scheme, Mechanics of Materials 84 (0) (2015) 28 – 43.

[9] V. I. Kushch, I. Sevostianov, V. S. Chernobai, Effective conductivity of composite with imperfect contact between elliptic fibers and matrix: Maxwells homogenization scheme, International Journal of Engineering Science 83 (0) (2014) 146 – 161.

[10] I. Sevostianov, G. Mishuris, Effective thermal conductivity of a composite with thermo-sensitive constituents and related problems, International Journal of Engineering Science 80 (0) (2014) 124 – 135.

[11] R. W. Zimmerman, Thermal conductivity of fluid-saturated rocks, Journal of Petroleum Science and Engineering 3 (3) (1989) 219 – 227.

[12] A. Giraud, I. Sevostianov, Micromechanical modeling of the effective elastic properties of oolitic limestone, International Journal of Rock Mechanics and Mining Sciences 62 (0) (2013) 23 – 27.

[13] F. Chen, I. Sevostianov, A. Giraud, D. Grgic, Evaluation of the effective elastic and conductive properties of materials containing concave pores, International Journal of Engineering Science 93 (2015) .. – ..

[14] E. Kazatchenko, M. Markov, A. Mousatov, Simulation of acoustic velocities, electrical and thermal conductivities using unified pore-structure model of double-porosity carbonate rocks, Journal of Applied Geophysics 59 (1) (2006) 16 – 35.

[15] E. Kazatchenko, M. Markov, A. Mousatov, E. Pervago, Joint inversion of conventional well logs for evaluation of double-porosity carbonate formations, Journal of Petroleum Science and Engineering 56 (4) (2007) 252–266.

[16] M. Markov, A. Mousatov, E. Kazatchenko, Conductivity of carbonate formations with microfracture systems, Journal of Petroleum Science and Engineering 69 (3-4) (2009) 247–254.

[17] M. Markov, A. Mousatov, E. Kazatchenko, I. Markova, Determination of electrical conductivity of double-porosity formations by using generalized differential effective medium approximation, Journal of Applied Geophysics 108 (0) (2014) 104 – 109.

[18] A. Aquino-López, A. Mousatov, M. Markov, E. Kazatchenko, Modeling and inversion of elastic wave velocities and electrical conductivity in clastic formations with structural and dispersed shales, Journal of Applied Geophysics 116 (0) (2015) 28 – 42.

[19] M. P. Lutz, R. W. Zimmerman, Effect of an inhomogeneous interphase zone on the bulk modulus and conductivity of a particulate composite, International Journal of Solids and Structures 42 (2005) 429–437.

[20] M. G. Alishaev, I. M. Abdulagatov, Z. Z. Abdulagatova, Effective thermal conductivity of fluid-saturated rocks: Experiment and modeling, Engineering Geology 135136 (2012) 24 – 39.

[21] J. ThomasJr, R. R. Frost, R. D. Harvey, Thermal conductivity of carbonate rocks, Engineering Geology 7 (1) (1973) 3 – 12.

[22] P. Suquet, M. Bornert, Rappels de calcul tensoriel et d'élasticité, in: Homogénéisation en mécanique des matériaux 2. Comportements non linéaires et problèmes ouverts, Hermes, Paris, 2001, pp. 171–202.

[23] J. Côté, J.-M. Konrad, Assessment of structure effects on the thermal conductivity of two-phase porous geomaterials, International Journal of Heat and Mass Transfer 52 (34) (2009) 796 – 804.

[24] M. Markov, V. Levin, A. Mousatov, E. Kazatchenko, Effective thermal conductivity of inhomogeneous medium containing gas-filled inclusions, Submitted to Special Issue: Mathematical methods in micromechanics in Mathematical Methods in the Applied Sciences - (-) (2015) –.

[25] S. Torquato, Random Heterogenous Materials. Microstructure and Macroscopic Properties, Springer-Verlag, 2002.

[26] J. Carslaw, H. Jaeger, Conduction of Heat in Solids, Oxford University Press, England, 1959.

[27] I. Sevostianov, A. Giraud, Generalization of Maxwell homogenization scheme for elastic material containing inhomogeneities of diverse shape, International Journal of Engineering Science 64 (0) (2013) 23 – 36.

[28] J. Sterpenich, J. Sausse, J. Pironon, A. Gehin, G. Hubert, E. Perfetti, D. Grgic, Experimental ageing of oolitic limestones under CO2 storage conditions. Petrographical and chemical evidence, Chemical Geology 265 (1-2) (2009) 99–112.

[29] A. Giraud, I. Sevostianov, Micromechanical modeling of the effective elastic properties of oolitic limestone, International Journal of Rock Mechanics and Mining Sciences 62 (0) (2013) 23 – 27.

[30] G. Vasseur, F. Brigaud, L. Demongodin, Thermal conductivity estimation in sedimentary bassins, Tectonophysics 224 (1995) 167–174.

[31] Y. Guéguen, T. Chelidze, M. L. Ravalec, Microstructures, percolation thresholds, and rock physical properties, Tectonophysics 279 (1) (1997) 23–35.

[32] C. Clauser, E. Huenges, Thermal conductivity of rocks and minerals, in: A Handbook of Physical Constants: Rock Physics and Phase Relations, vol.3, ed. Tom Ahrens, The American Geophysical Union, 105-126 (1995).

[33] D. Bruggeman, Berechnung verschiedner Physicalischer Konstanten von heterogenen Subztanzen. I. Dielektrizitätskonstanten und Leitfähigkeiten der Mischkörper aus isotropen Substanzen, Annalen der Phyzik 416 (7) (1935) 636–664.

[34] F. Chen, A. Giraud, I. Sevostianov, D. Grgic, Numerical evaluation of the Eshelby tensor for a concave superspherical inclusion, International Journal of Engineering Science 93 (2015) 51–58.

[35] E. C. Robertson, Thermal properties of rocks, Tech. rep., Open File Report No. 88-441, U.S. Geological Survey (1988).

[36] Y. Popov, V. Tertychnyi, R. Romushkevich, D. Korobkov, J. Pohl, Interrelations Between Thermal Conductivity and Other Physical Properties of Rocks: Experimental Data, Pure and Applied Geophysics 160 (5-6) (2003) 1137–1161.

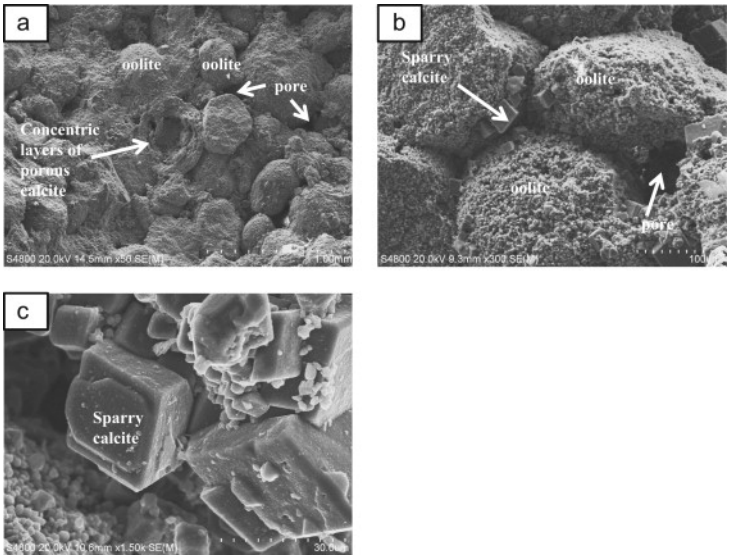

1

Figure 1: Scanning Electron Microscopy (SEM) images of Lavoux limestone (see [29])

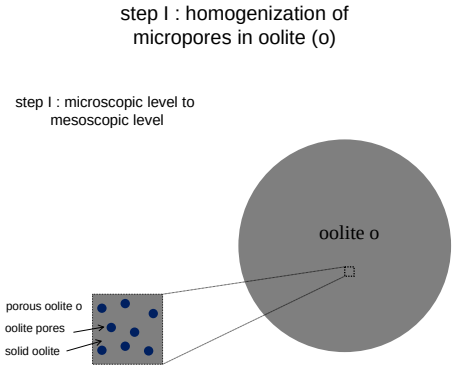

Figure 2: First homogenization step: micropores inside oolite core are homogenized by using self consistent method (2D representation of a 3D microstructure)

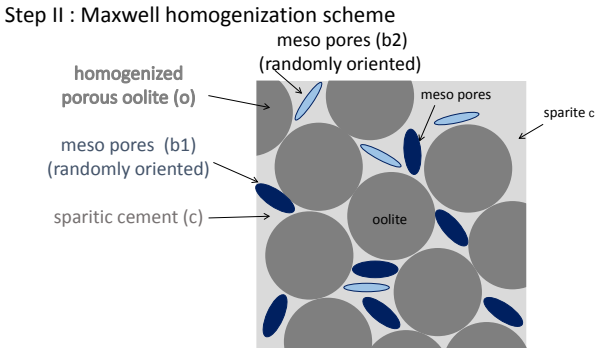

Figure 3: Second homogenization step: transition from mesoscale to macroscale with Maxwell homogenization method, case of simplified model (ellipsoidal approximation for all the pores)

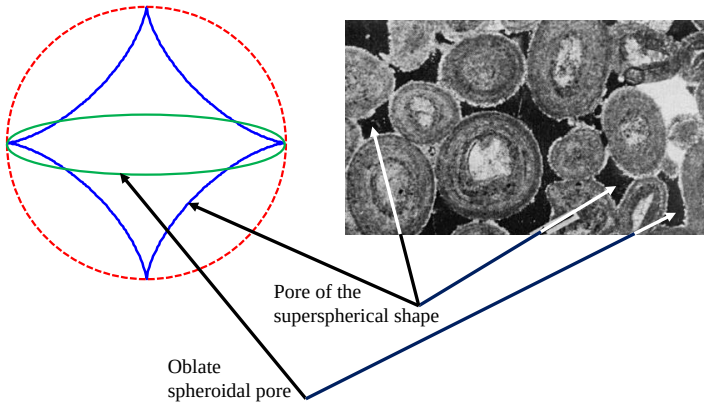

Figure 4: Mesoporosity: ellipsoidal pores ($b1$) and concave pores ($b2$) (see [29])

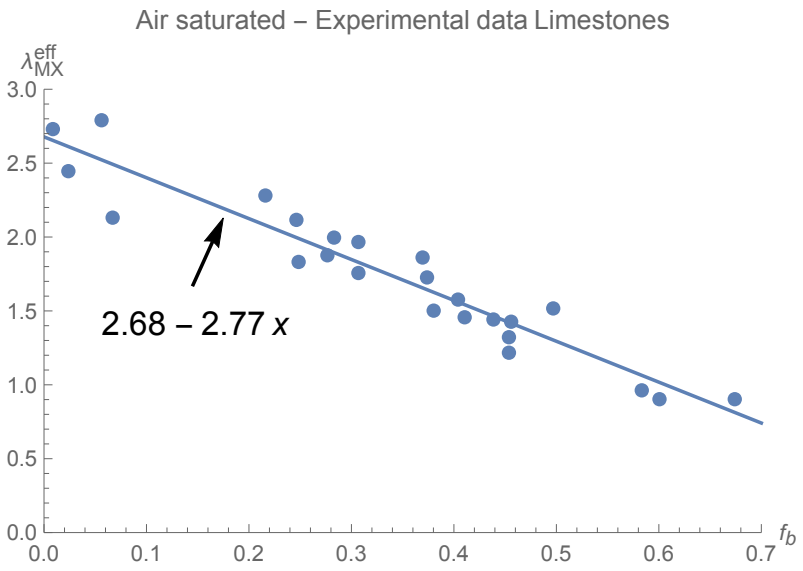

Figure 5: Pores saturated with air: experimental thermal conductivity as a function of porosity, for pure calcitic limestones [35]

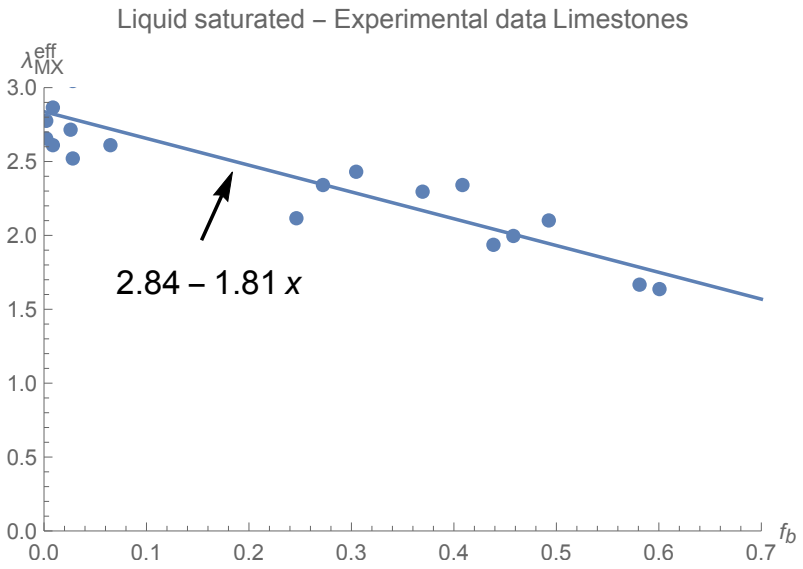

Figure 6: Pores saturated with water liquid: experimental thermal conductivity as a function of porosity, for pure calcitic limestones [35]

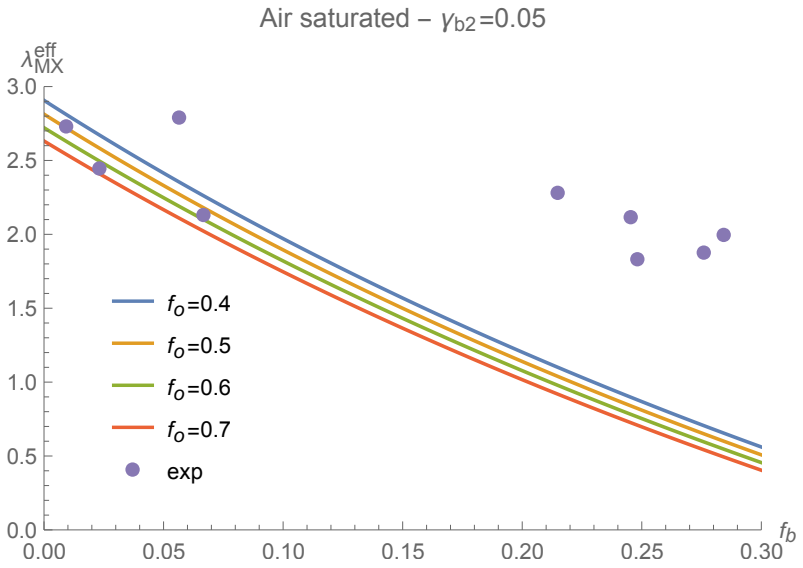

Figure 7: Pores saturated with air : effective thermal conductivity as a function of meso-porosity with $b2$ = random distribution of cracks (oblate $\gamma = 0.05$)- blue : $f_o = 0.4$ - $f_o = 0.5$ - green : $f_o = 0.6$ - red : $f_o = 0.7$, experimental data taken from [35]

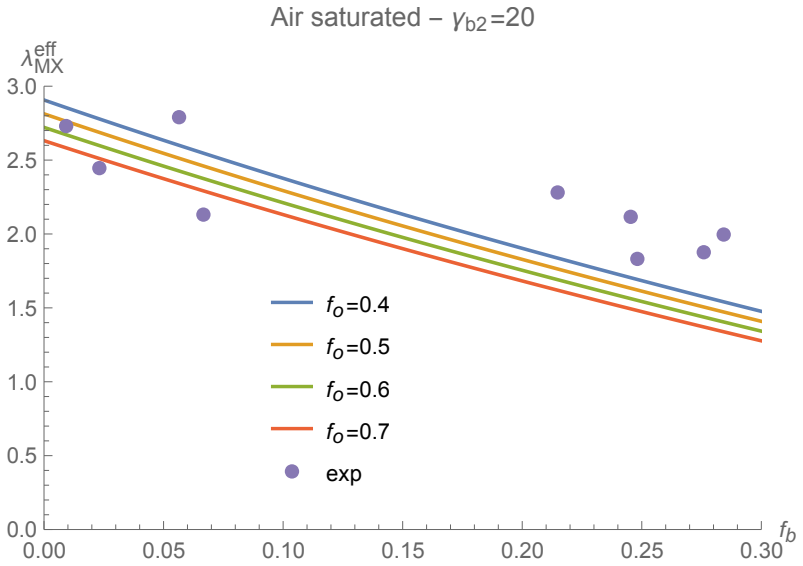

Figure 8: Pores saturated with air : effective thermal conductivity as a function of mesoporosity with $b2$ = random distribution of needles (prolate $\gamma = 20$)- blue : $f_o = 0.4$ - $f_o = 0.5$ - green : $f_o = 0.6$ - red : $f_o = 0.7$, experimental data taken from [35]

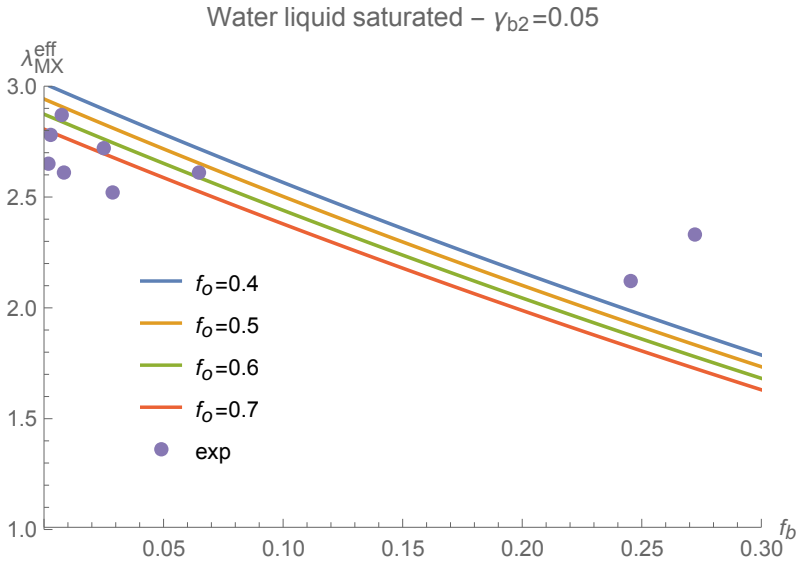

Figure 9: Pores saturated with liquid water : effective thermal conductivity as a function of mesoporosity with $b2$ = random distribution of cracks (oblate $\gamma = 0.05$)- blue : $f_o = 0.4$ - $f_o = 0.5$ - green : $f_o = 0.6$ - red : $f_o = 0.7$, experimental data taken from [35]

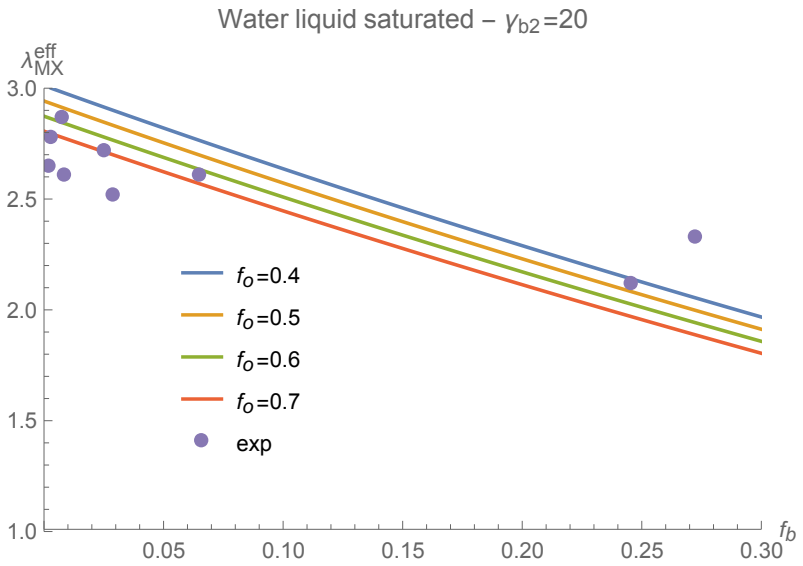

Figure 10: Pores saturated with liquid water : effective thermal conductivity as a function of mesoporosity with $b2$ = random distribution of needles (prolate $\gamma = 20$)- blue : $f_o = 0.4$ - $f_o = 0.5$ - green : $f_o = 0.6$ - red : $f_o = 0.7$, experimental data taken from [35]

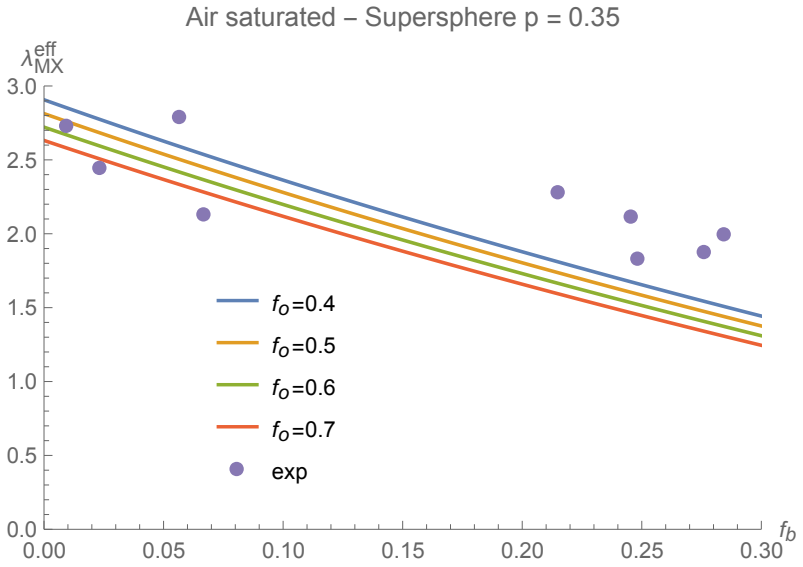

Figure 11: Pores saturated with air : effective thermal conductivity as a function of mesoporosity with $b2$ = random distribution of superspheres ($p = 0.35$) - blue : $f_o = 0.4$ - $f_o = 0.5$ - green : $f_o = 0.6$ - red : $f_o = 0.7$, experimental data taken from [35]

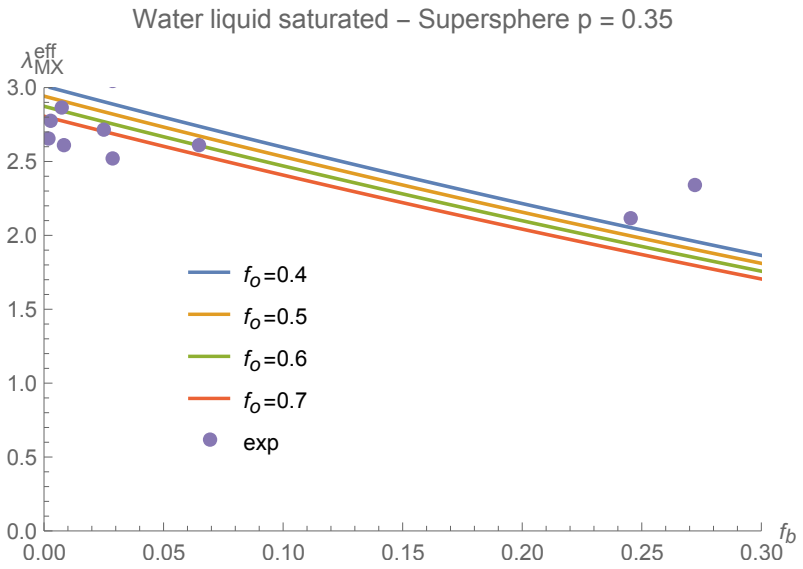

Figure 12: Pores saturated with liquid water : effective thermal conductivity as a function of mesoporosity with $b2$ = random distribution of superspheres ($p = 0.35$) - blue : $f_o = 0.4$ - $f_o = 0.5$ - green : $f_o = 0.6$ - red : $f_o = 0.7$, experimental data taken from [35]

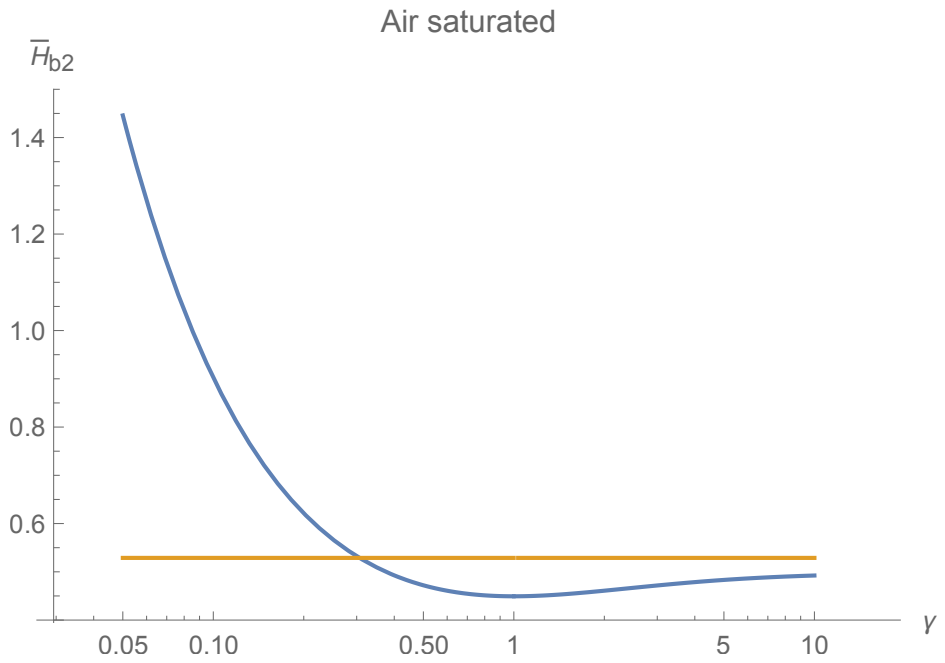

Figure 13: Pores saturated with air: Resistivity contribution tensor of spheroid as a function of pore aspect ratio γ, comparison with supersphere ($p = 0.35$, $\overline{H}_{b2}^{\mathrm{SP}-air} = 0.529$)

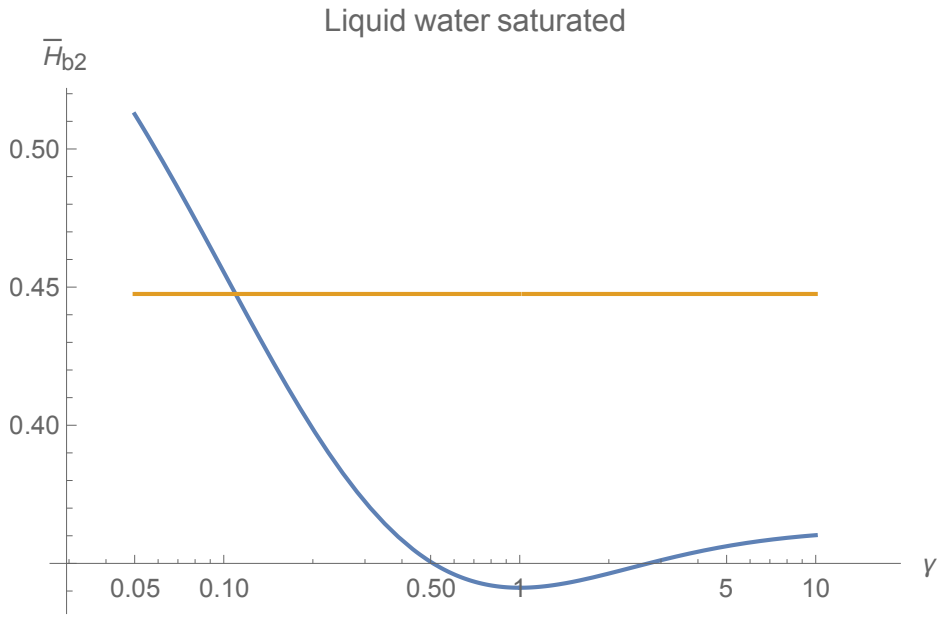

Figure 14: Pores saturated with liquid water : Resistivity contribution tensor of spheroid as a function of pore aspect ratio γ, comparison with supersphere ($p = 0.35$, , $\overline{H}_{b2}^{\mathrm{SP}-lq} = 0.448$)